Hindawi Publishing Corporation
Journal of Nanomaterials
Volume 2014, Article ID 703072, 9 pages
http://dx.doi.org/10.1155/2014/703072

Research Article

Effect of Mn-Site for Al Substitution on Structural, Electrical and Magnetic Properties in $La_{0.67}Sr_{0.33}Mn_{1-x}Al_xO_3$ Thin Films by Sol-Gel Method

H. Abdullah,[1] M. Syafiq Zulfakar,[1] and S. Kien Chen[2]

[1] *Department of Electrical, Electronic and Systems Engineering, Faculty Engineering and Built Environment, Universiti Kebangsaan Malaysia, 43600 Bangi, Selangor, Malaysia*
[2] *Physics Department, Faculty of Sciences, Universiti Putra Malaysia, 43400 Serdang, Selangor, Malaysia*

Correspondence should be addressed to H. Abdullah; huda@eng.ukm.my

Received 10 October 2013; Revised 14 January 2014; Accepted 28 January 2014; Published 26 March 2014

Academic Editor: Wanqin Jin

Nanocrystalline $La_{0.67}Sr_{0.33}Mn_{1-x}Al_xO_3$ ($x = 0.00, 0.05, 0.10, 0.15, 0.20$, and 0.25) thin films have been prepared on quartz substrates by sol-gel method. The structural and morphology studies were investigated via X-ray diffraction (XRD) and field emission scanning electron microscope (FESEM). XRD graph patterns show rhombohedral distorted perovskite structures. FESEM images show that the average grain size decreased as the concentration of x increased. Electrical property was investigated using four-point probe technique. Resistivity results show that metal-insulator transition (MIT) temperatures (T_p) decreased when the concentration of x increased. T_p shifted to lower temperature when the concentration of x increased. The data was analyzed based on theoretical models, where the ferromagnetic resistivity is followed with the equation $\rho = \rho_o + \rho_2 T^2$, where ρ_o is due to the significance of grain boundary effects and a second-term $\sim \rho_2 T^2$ appears that might be applied to the electrons scattering. In the high temperature regime ($T > T_p$), the resistivity data can be well described by small polaron hopping (SPH) and variable range hopping (VRH) mechanisms. Magnetic property was investigated using a vibration sample magnetometer. All samples that were obtained showed hysteresis curve with the highest value of magnetization for sample $x = 0.10$.

1. Introduction

The discovery of the colossal magnetoresistance (CMR) effect in epitaxial thin films of $Ln_{1-x}R_xMnO_3$ perovskite manganites, where R is alkaline earth elements and Ln is rare-earth element, gives an effect for usage in data storage and sensing application [1, 2]. Bulk compound is typically different with the properties of CMR thin films where in bulk compounds, doping concentration can change the CMR effects [3].

Perovskite-type lanthanum strontium manganate $La_{0.65}Sr_{0.35}MnO_3$ exhibits colossal magnetoresistance (CMR) with Curie temperature more than 370 K, where it can be operated at a room temperature [4]. The manganese oxide not only showed a metallic conduction below Curie temperature T_c but also enhanced the ferromagnetic interaction when La^{3+} ions are replaced with alkaline earth elements or also known as divalent metal ions (Ca^{2+}, Sr^{2+}, Ba^{2+}) in perovskite oxide structures [5]. By comparing to between Ln site with R site doping will not only modify the crucial Mn^{3+}–O^{2-}–Mn^{4+} interaction that will bring many complicated between Mn ions and dopands [6]. These compounds are Mn^{3+} and Mn^{4+} ions, which play an important part in double-exchange interaction when substituted with metallic resistivity. Distortion of John-Teller effect could give different result for transport properties, which removes the double degeneracy of Mn in e_g orbital and provides a mechanism for coupling among the electronic, magnetic and lattice degrees of freedom [7].

The aim for this work is to investigate the effect of substituting Al at Mn sites with the structural and electrical properties of $La_{0.67}Sr_{0.33}Mn_{1-x}Al_xO_3$ samples with $x = 0.00$, 0.05, 0.10, 0.15, 0.20, and 0.25.

2. Experimental Details

$La_{0.67}Sr_{0.33}Mn_{1-x}Al_xO_3$ samples were prepared by using sol-gel method. The amounts of $La(NO_3)_3 \cdot H_2O$, $Sr(NO_3)_2$, $Mn(NO_3)_2$ and Al_2O_3 were weighed accurately and dissolved in aqueous solutions that were added into deionized water, nitric acid, and triethanolamine (TEA). The produced solutions were dissolved completely and were stirred and heated at 90°C for 3 h to evaporate the excess solvent and water. Quartz substrate with dimensions (10 mm × 10 mm) was washed with acetone and methanol. The clean substrates were rinsed with distilled water and dried. All samples were deposited on the quartz substrate by using spin coating technique. The produced solutions were spin coated with 5 layers onto the substrate with 900 rpm for 25 s for each coating. All samples were annealed with temperature at 650°C for 1 h with heating and cooling rates of 1°C/min. The flowchart of the preparation of LSMOA thin film samples as shown in Figure 1. The morphological structures were investigated using X-ray diffraction (XRD) and field emission scanning electron microscope (FESEM). Electrical property was investigated using 4-point probe technique within temperature range of 200–300 K. The magnetic property was investigated using a vibration sample magnetometer (VSM) analysis at room temperature with a magnetic field range of −10 kOe to +10 kOe. All experimental results were characterized by good repeatability.

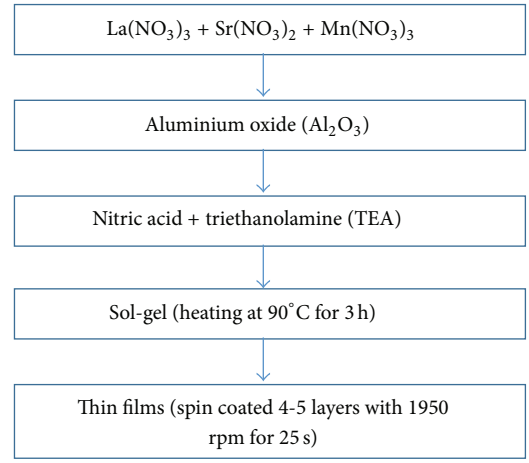

Figure 1: Flowchart for the preparation of LSMAO sol-gel and thin films.

3. Results and Discussion

Field emission scanning electron microscope (FESEM) analysis was used to investigate the morphological structure of $La_{0.67}Sr_{0.33}Mn_{1-x}Al_xO_3$ thin film samples with different concentrations of x. Based on Figure 2, the clear image of grain was observed at $x = 0.10$ compared to the other samples. Based on the average grain size of the sample that was measured during the SEM analysis, it shows that when the concentration of x is increased, the size of grain decreased. Structural morphology of $La_{0.67}Sr_{0.33}Mn_{1-x}Al_xO_3$ samples becomes more compact and homogenous when the concentration of x increased. The grain size of all samples was observed with round shape, but for sample ($x = 0.00$) it is shown that the particles are submerged between each other. Similar finding has also reported that, by increasing the concentration, the nanoparticles were tightly tied together and the size of the particles reduced for sample $La_{0.67}Ba_{0.33}(Mn_{1-x}Al_x)O_3$ [8]. This was also reported by Abdullah and Halim [9], where the reduction of size and linkage between the particles can be clearly seen, as the samples were doped for several concentrations. Based on Figure 3, it shows the graph of particles size against concentration. The grain sizes decreased as the concentration of x increased. The reduction size of Al plays the main role where the Al^{3+} ion is smaller than Mn^{3+}/Mn^{4+} ion. This indicates that more Al^{3+} ions will be substituted or take place in Mn^{3+}/Mn^{4+} ion.

Morphological structure of $La_{0.67}Sr_{0.33}Mn_{1-x}Al_xO_3$ thin film samples, with concentration of $x = 0.00$, 0.05, 0.10, 0.15, 0.20, and 0.25, was characterized using XRD analysis. XRD graph pattern indicates no clear formation of single phase with rhombohedral distorted perovskite structures as shown in Figure 4. Sahu et al. [10] have reported that the formation of LSMO phase calcined at 600°C. There are several peaks observed with Miller indices (104) and (111) plane at $2\theta = 32.68°$, 38.24°, and 39.96°. These indicate that LSMAO thin film samples for $x = 0.05$ and $x = 0.20$ have a fine crystal structure compared with other samples. The intensity of the width diffraction decrease when the concentration of x increased. This showed that when the level of doping increased, it may have effect on the crystal structures of the LSMAO sample.

Figure 5 shows a resistivity, ρ of the $La_{0.67}Sr_{0.33}Mn_{1-x}Al_xO_3$ systems. All samples show a peak of a resistivity curve where it has the highest resistivity at the particular temperature which was known as peak temperature (T_p). According to the plot, it shows that when the temperature increases, the resistivity value decreases. This indicates a semiconducting behavior. All samples follow the metal-insulator transition (MIT) at T_p. In a metallic region, in a semiconducting region the plot slightly decreases. Based on the plot, T_p should shifted at lower temperature for samples $x = 0.00$ and 0.05, but for sample $x = 0.10$, 0.20 and 0.25 showing otherwise. Figure 6 shows the schematic dependents of the peak resistivity temperature (T_p) on the Al concentration. This phenomenon indicates the electron hopping between Mn^{3+} and Mn^{4+} ions. As a result, double exchange has been suppressed as the concentration increased. This result indicates the weakened double exchange (DE) ferromagnetic interactions. It shows that when the concentration of increased, peaks of resistivity decreased from $x = 0.00$ to 0.05 and for samples $x = 0.15$, 0.20, and 0.25 increased, respectively, and do not follow the theory of double exchange (DE) ferromagnetic interactions. Peak temperature, T_p, shifted to lower temperature when the concentration of x increased because of the charge transfer mechanisms of Mn^{3+}–O^{2-}–Mn^{4+} network which has been replaced with Mn^{3+}–O^{2-}–Al^{4+}. This finding has also been reported by Abdullah et al. [11] as when the concentration of

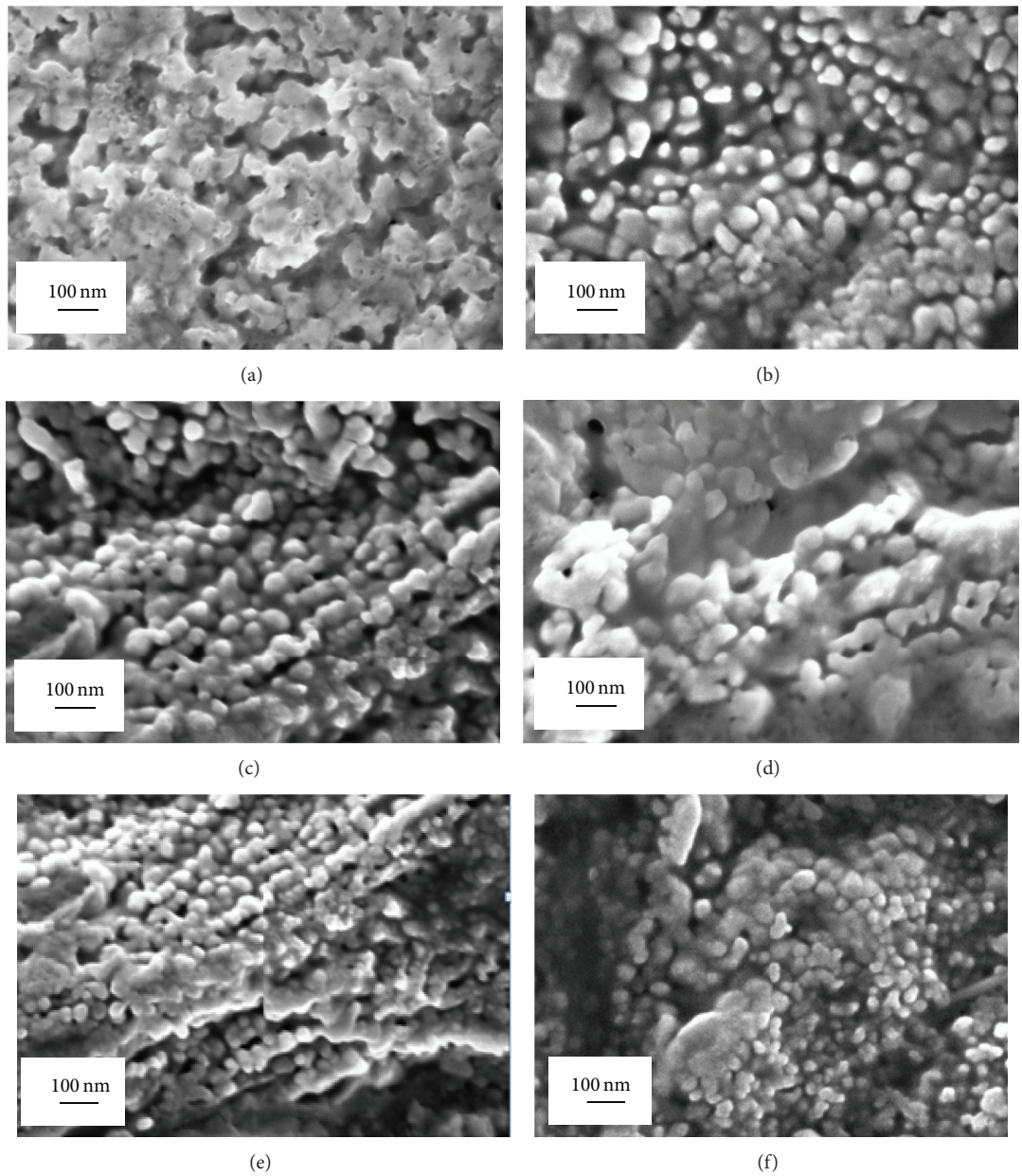

FIGURE 2: FESEM image of $La_{0.67}Sr_{0.33}Mn_{1-x}Al_xO_3$ with different concentrations of (a) $x = 0.00$, (b) $x = 0.05$, (c) $x = 0.10$, (d) $x = 0.15$, (e) $x = 0.20$, and (f) $x = 0.25$.

Al increased, this may affect the charge transfer mechanism. This is obviously because of replacing conducting regions of a conducting matrix by insulating regions.

Figure 7 shows plotted graph for resistivity data against temperature. Below T_p, according to double exchange theory, the mechanism of electronic conduction can be applied. The Mn^{3+}–O–Mn^{4+} coupling allows conduction through charge transfer from half-filled to empty e_g orbital. In this regime, the metallic behavior of the samples can be explained in terms of electron-magnon scattering of the carriers. The resistivity data fit quite well with the following expression:

$$\rho = \rho_o + \rho_2 T^2, \quad (1)$$

where the first term ρ_o corresponds to the resistivity arising due to domain, grain boundary, and other temperature independent scattering mechanisms. The second term $\rho_2 T^2$ appears as a result of electron-magnon scattering in ferromagnetic phase. Based on Table 1, the values of parameters ρ_2 increased with the disorder increment as values of ρ_2 for $x = 0.10$ and 0.15 decreased and the values for $x = 0.20$ increased. As the concentration of doping increased, the value of ρ_2 should increase due to the suppression of spin fluctuation. Thus, the spin scattering cannot be neglected in this regime as the measured data can be best explained by electron-magnon scattering. The best fitted parameters are given in Table 1. It is noted that the values of both ρ_o and ρ_2 increase with the

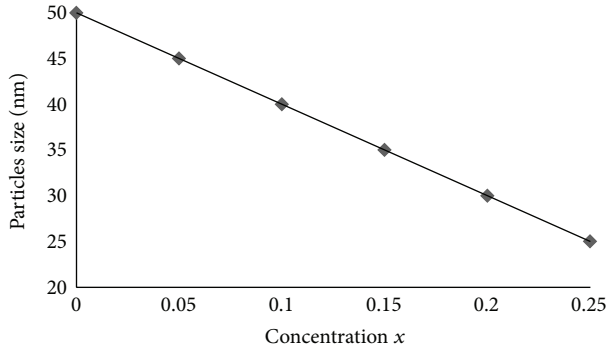

FIGURE 3: Particle size of $La_{0.67}Sr_{0.33}Mn_{1-x}Al_xO_3$ as a function of concentration x.

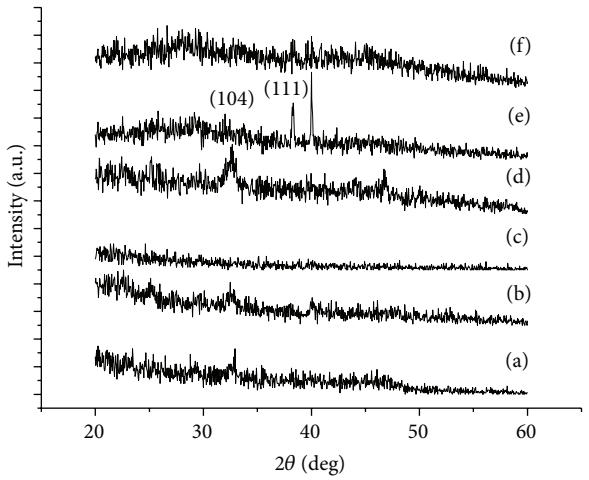

FIGURE 4: XRD patterns of $La_{0.67}Sr_{0.33}Mn_{1-x}Al_xO_3$ with different concentrations of (a) $x = 0.00$, (b) $x = 0.05$, (c) $x = 0.10$, (d) $x = 0.15$, (e) $x = 0.20$, and (f) $x = 0.25$.

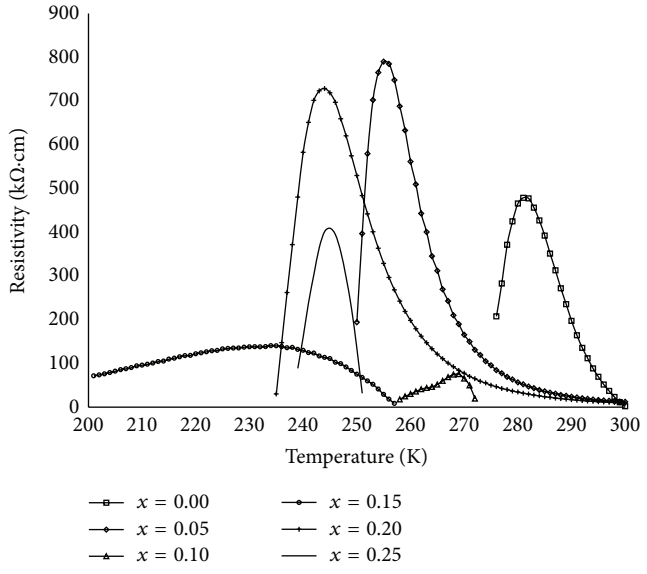

FIGURE 5: The temperature dependence of resistivity for $La_{0.67}Sr_{0.33}Mn_{1-x}Al_xO_3$ with concentration; (a) $x = 0.00$, (b) $x = 0.05$, (c) $x = 0.10$, (d) $x = 0.15$, (e) $x = 0.20$, and (f) $x = 0.25$.

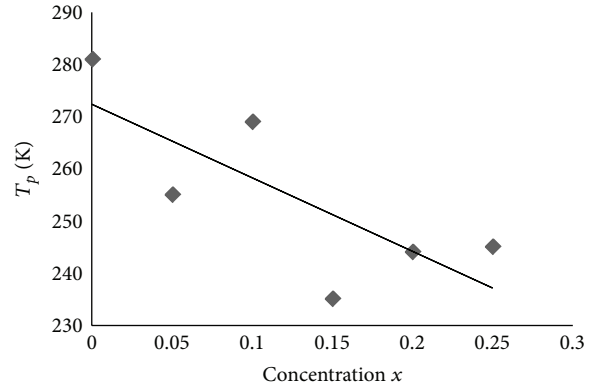

FIGURE 6: Peak resistivity temperature, (T_p), as a function of concentration x.

increase of x. As the doping increases, the size of the domain boundary decreases and ρ_o becomes larger. It means that both these parameters are increasing with decreasing grain size, which may be an evidence for increasing the scattering processes due to the reduction of grains of the material. Thus decreasing the grain size may increase the grain boundary region and hence the net grain boundary scattering term as well as electron-magnon scattering term. Therefore, grain boundary plays a dominant role in the conduction process, and it acts as the region of reduced scattering centre for conduction electron. The increase of ρ_2 with x is due to spin fluctuation [9].

3.1. The High-Temperature ($T > T_p$) Regime. The high-temperature electronic transport properties among these materials may be divided into 2 distinct phenomena based on 2 different models, each one predicting different temperature dependence for the resistivity. For example, to explain the conduction just above T_p, the variable range hopping (VRH) model has been suggested, while the small polaron hopping model is considered at temperatures beyond $\theta_D/2$ (where θ_D is the Debye temperature). In the latter case, a polaron can be thought to be trapped inside a local energy well of height E_a and, when the field is applied, one side of the well is lowered slightly with respect to the other. This makes the polaron likely to hop more in that direction [11–13].

3.1.1. Variable Range Hopping (VRH) Model ($T_p < T < \theta_D/2$). The samples show semiconducting-like behaviors for $T > T_p$ ($d\rho/dT < 1$). The transport data in the semiconducting regime of $(Pr_{1-x}Nd_x)_{2/3}Ba_{1/3}MnO_3$ compounds have been analysed by the Mott variable range hopping (Mott-VRH) model [14], according to equation

$$\sigma = \sigma_0 \exp\left(\frac{T_o}{T}\right)^{1/4}, \quad (2)$$

where ρ_o is a preexponential factor, T_o is a constant [$= 16\alpha^3/k_B N(E_F)$], and $N(E_F)$ is the density of state (DOS) at the Fermi level, which is calculated from the slope of the log σ versus $T^{-1/4}$ curves shown in Figure 8.

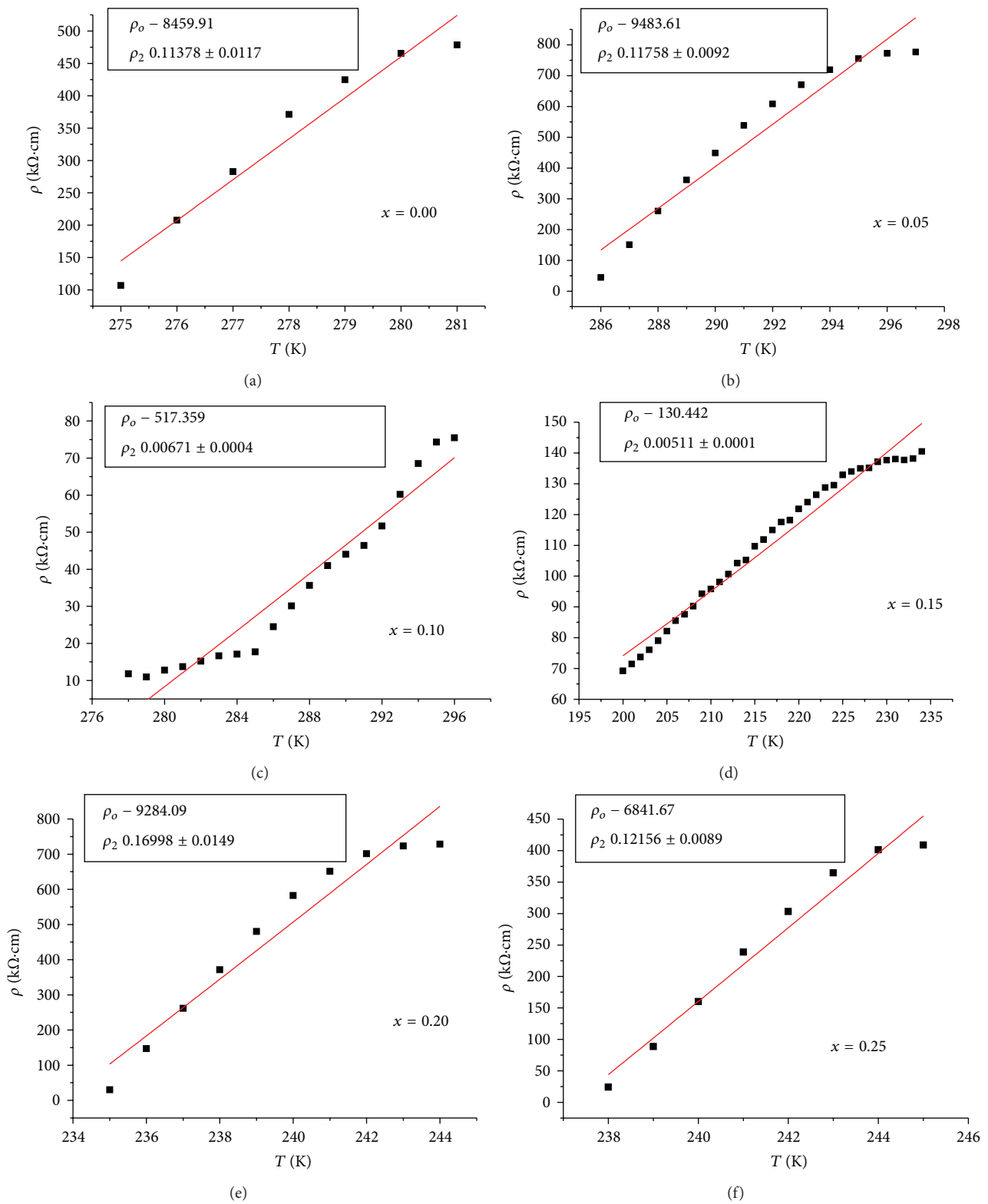

FIGURE 7: Resistivity data showing T^2 dependence for $La_{0.67}Sr_{0.33}Mn_{1-x}Al_xO_3$ system. Solid lines are the best fit with equation $\rho = \rho_o + \rho_2 T^2$.

Table 1: Best fitted parameters obtained from the fitting of the low temperature resistivity data in the metallic regime of $La_{0.67}Sr_{0.33}Mn_{1-x}Al_xO_3$ manganites with $\rho = \rho_o + \rho_2 T^2$.

Concentration x	ρ_o (Ωcm K^{-2})	ρ_2 (Ωcm K^{-2})
0.00	−8459.91	0.11378
0.05	−9483.61	0.11758
0.10	−9284.09	0.00671
0.15	−6841.67	0.00511
0.20	−517.36	0.16998
0.25	−130.44	0.12156

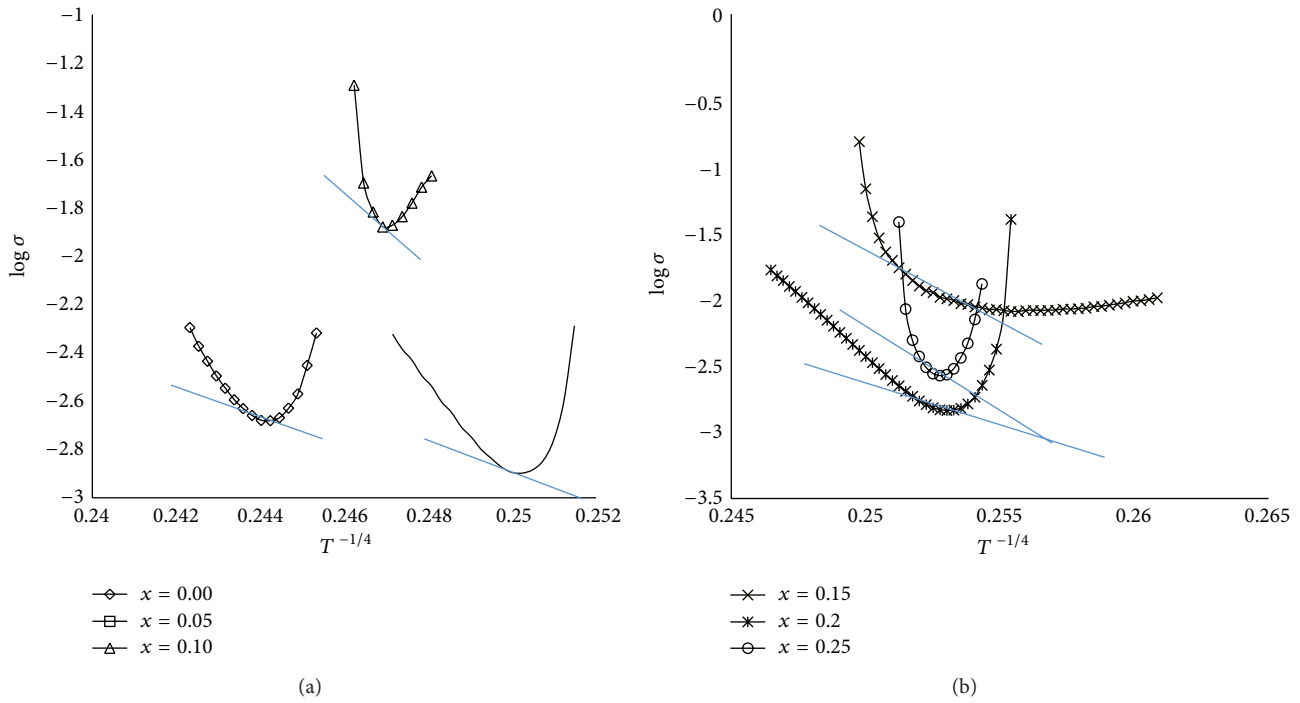

Figure 8: The slope of the log σ versus $T^{-1/4}$ curves.

Equation (2) is used to explain the conductivity data at temperatures for which $T_p < T < \theta_D/2$. From the resistivity data, it can be seen that temperatures above T_p are fitted by plotting log(σ) versus $T^{-1/4}$. $\theta_D/2$ values or it can be estimated based on the graph for $\theta_D/2 \approx T^{-1/4}$, where deviation from linearity occurs in the temperature region above T_p. T_o values for each of the samples were calculated from the slopes of log(σ) versus $T^{-1/4}$. Finally, using the T_o values, $N(E_F)$, the Fermi level for each material was also obtained. All of the values that were obtained are presented in Table 2. For the samples with higher resistivity values, the VRH region becomes smaller. At the high temperature ($T > \theta_D/2$), conductivity data are better fitted with the small polaron hopping (SPH) model.

3.1.2. Small Polaron Hopping Model ($T > \theta_D/2$). For the conduction mechanism of these materials at high temperatures ($T > \theta_D/2$), the resistivity data of the Al-doped and undoped LSMO films can be well fitted with the thermally activated small polaron hopping (SPH) model of Mott, given by equation

$$\rho = \rho_\alpha T \exp\left(\frac{E_a}{k_B T}\right), \tag{3}$$

where ρ_α is the residual resistivity and E_a is the activation energy. ν_{ph} is the optical phonon frequency and can be estimated from the relation $h\nu_{ph} = K_B\theta_D$. The resistivity has been replotted as ln(ρ/T) versus $1/T$, and, from the slope of the curve, the activation energy, E_a, can be estimated (using Table 3). The plots are shown in Figure 9. Table 2 also shows the value of the phonon frequency against the concentration, x. It indicates that the frequency of the lattice wave decreases with increasing Nd content. As the concentration of Nd increased, the vibrational energy in periodic solids decreased.

Jung [15] suggested that higher values (2 to 3 orders than those of the usual oxide semiconductors) for the $N(E_F)$ of the present manganite system could be due to the high values of conductivity. Furthermore, these higher values of $N(E_F)$ are clear signatures of the applicability of adiabatic small

Table 2: Values of $\theta_{D/2}$, phonon frequency, ν (Hz), the density of states, $N(E_F)$, at Fermi level, and the activation energies from the resistivity plot.

x	T_pT_p (K)	T_o	$N(E_F)$ (eV^{-1} cm^{-3}) $\times 10^{16}$	$\theta_D/2$	ν (Hz) $\times 10^{12}$	E_a (meV)
0.00	282	37428689.3	5.4267	284.0283	5.9183	977.521
0.05	256	46396954.9	4.3777	258.003	5.3759	711.172
0.10	270	2798410000	0.07258	271.001	5.6469	867.893
0.15	233	280200294	0.72489	252.000	5.2509	1448.356
0.20	244	1600000000	0.01269	247.003	5.1468	1760.435
0.25	245	9927117782	0.0204	249.003	5.1885	3019.785

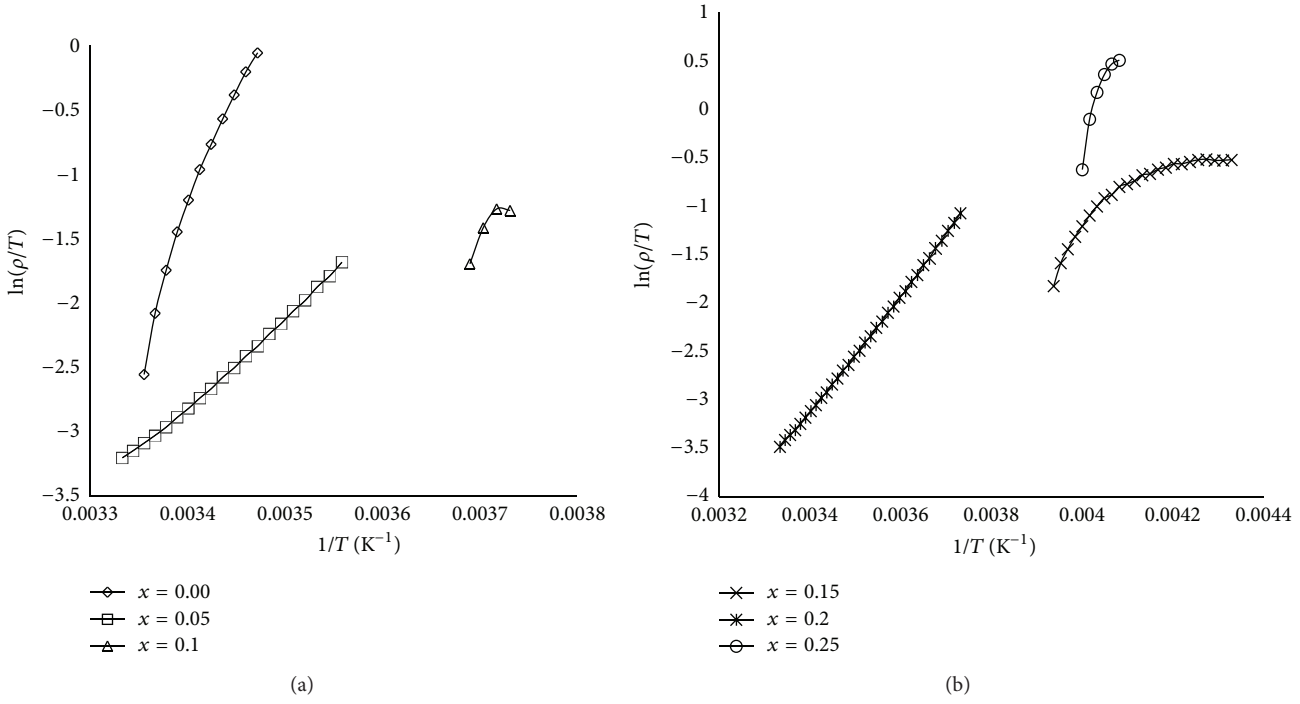

Figure 9: Plot of ln ρ/T versus $1/T$ for $La_{0.67}Sr_{0.33}Mn_{1-x}Al_xO_3$.

Table 3: Value of magnetization with concentration of Al at 10 kOe, measured at room temperature.

Concentration x	Magnetization (emu/g)
0.00	0.0457
0.05	0.1855
0.10	0.0287
0.15	0.1293
0.20	0.0537
0.25	0.0717

polaron hopping mechanisms. Based on this fact, it has been concluded that the adiabatic small polaron hopping model explains the conduction mechanism of the samples used in the present investigation. Furthermore, it is also clear from Table 2 that the values of E_a are less for the first 2 samples as compared to the remaining 2 samples. This may be attributed to oxygen deficiency. In the case of the last 2 samples, the oxygen deficiency induces an increase in the bending of the Mn–O–Mn bond angle, thereby narrowing the bandwidth and enhancing the effective mass of the charge carrier. Due to this fact, the effective band gap increases with increasing oxygen deficiency. Therefore, higher values for the activation energies are needed for the charge carriers to overcome this band gap [16]. The activation energy (E_a) values increase [13] and decrease depending on the grain size, and the observed behaviour may be explained as follows. It is known that, with increasing grain size, the interconnectivity between grains, which enhances the possibility of conduction electrons to hop to neighbouring sites, increases [17], and the value of E_a decreases.

Magnetic property was investigated using a vibration sample magnetometer (VSM) at room temperature. All samples were measured by applying magnetic field in a range −10 kOe to +10 kOe. Figure 10 shows the hysteresis curve graph pattern for $La_{0.67}Sr_{0.33}Mn_{1-x}Al_xO_3$ sample

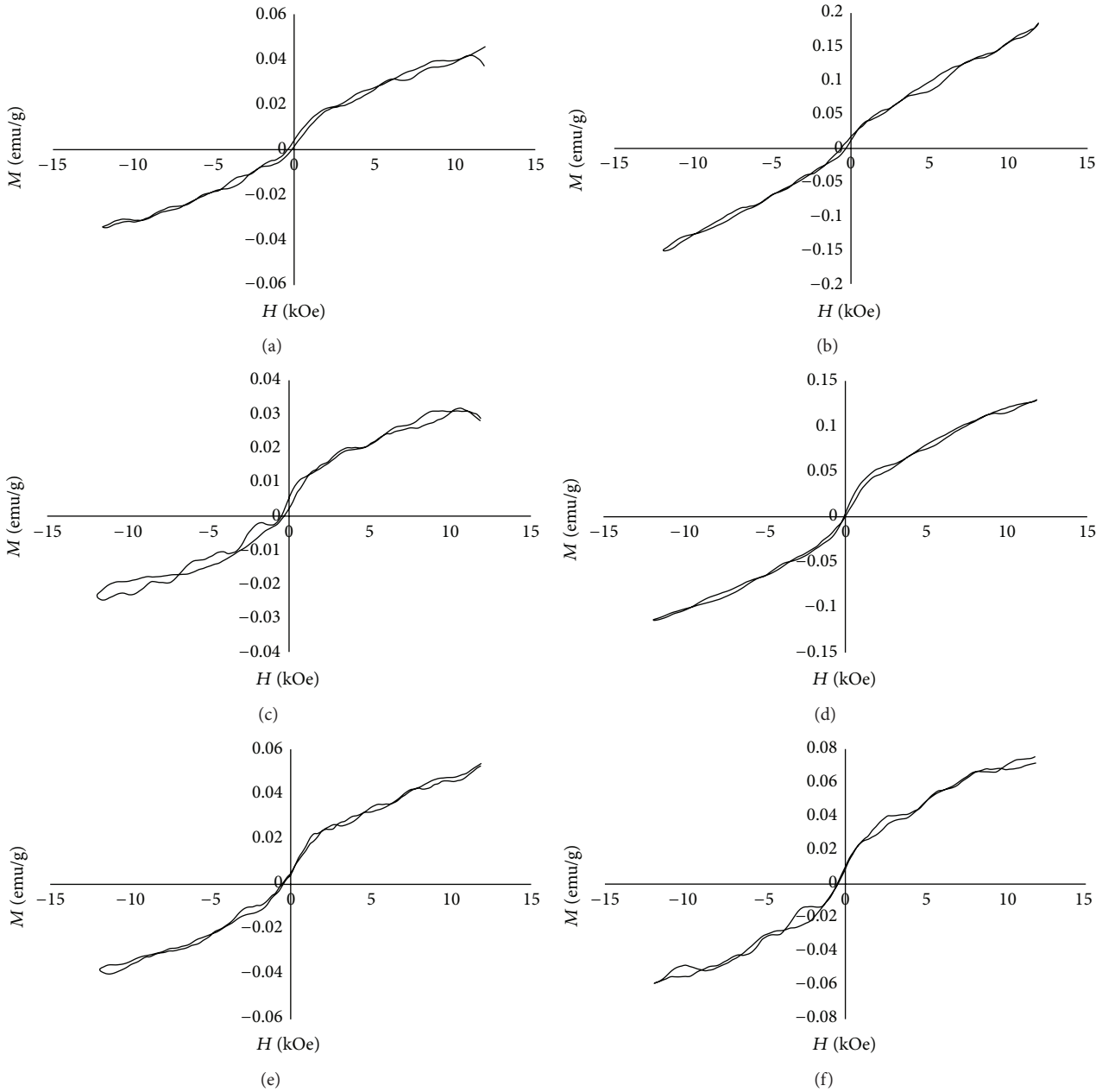

Figure 10: Vibration sample magnetometer (VSM) pattern of $La_{0.67}Sr_{0.33}Mn_{1-x}Al_xO_3$ thin film at room temperature with concentration of (a) $x = 0.0$, (b) $x = 0.05$, (c) $x = 0.10$, (d) $x = 0.15$, (e) $x = 0.20$, and (f) $x = 0.25$.

with concentration of $x = 0.00, 0.05, 0.10, 0.15, 0.20$, and 0.25. Graph pattern that was obtained was known as a magnetization curve or hysteresis curve. Based on Table 3, it indicates that the highest value of magnetization is for samples $x = 0.05$ and 0.15 where the values are 0.1855 emu/g and 0.12933 emu/g. Samples $x = 0.05$ and 0.15 show the highest value of magnetization compared to other samples, which indicates weak ferromagnetic properties. Different finding has reported LSMO particles that were prepared by sol-gel method. The magnetic properties show a good ferromagnetic behavior at room temperature which gives 29.60 emu/g. It indicates that the magnetic ordering of Mn^{3+} and Mn^{4+} ions in LSMO might be improved under the influence of a magnetic field [18]. The other samples may indicate the properties of weak paramagnetic due to the fact that the value of magnetization is low where the effect can only be measured by VSM analysis. The slope of *M-H* loop for samples $La_{0.67}Sr_{0.33}Mn_{1-x}Al_xO_3$ is not narrow where it was reported by Krishna and Venugopal Reddy [19] in which the loop width of PSMO, PPMO, and PBMO is narrow, which gives an impression that these three samples might have soft magnetic nature.

4. Conclusions

Nanocrystalline $La_{0.67}Sr_{0.33}Mn_{1-x}Al_xO_3$ (x = 0.00, 0.05, 0.10, 0.15, 0.20, and 0.25) thin film samples were successfully prepared on quartz substrates by sol-gel method prepared at room temperature. Based on SEM images, samples with Al^{3+} doped show a round shape and become more compact, when the composition of concentrations increased. XRD graph pattern of samples showed a single phase with rhombohedral distorted perovskite structures, where the highest peaks are (104) and (111). Temperature dependence shows that T_p is the influence by the concentration of x. Undoped sample gave the higher T_p compared to the others. T_p shifted to lower temperature when the concentration of x increased. Metallic conduction in these systems follows T^2 dependences, indicating the importance of electron-magnon contribution. The electrical conduction mechanism of these materials at low temperatures ($T < T_p$) may be due to the electron-magnon scattering processes. While, in the high temperature regime ($T > T_p$), the conduction can be explained by the variable range hopping (VRH) model and the small polaron hopping (SPH) mechanisms. SPH conduction is observed above the MIT temperature for all of the samples. Magnetic property shows a weak ferromagnetic property in magnetic field −10 kOe to +10 kOe.

Conflict of Interests

The authors declare that there is no conflict of interests regarding the publication of this paper.

Acknowledgments

The authors gratefully acknowledge IMEN, Universiti Kebangsaan Malaysia, for the permission to use all the facilities and the staff for the support to finish this paper. The Ministry of Higher Education (MOHE) is gratefully acknowledged for the Grant under FRGS vote: UKM-KK-07-FRGS0026-2009 (Growth of Nanostructured Colossal Magnetoresistive Material for Low-Field Magnetic Sensing Device).

References

[1] F. Tsui, M. C. Smoak, T. K. Nath, and C. B. Eom, "Strain-dependent magnetic phase diagram of epitaxial $La_{0.67}Sr_{0.33}MnO_3$ thin films," *Applied Physics Letters*, vol. 76, no. 17, pp. 2421–2423, 2000.

[2] A. J. Millis, T. Darling, and A. Migliori, "Quantifying strain dependence in "colossal" magnetoresistance manganites," *Journal of Applied Physics*, vol. 83, no. 3, pp. 1588–1591, 1998.

[3] J. Dho, W. S. Kim, and N. H. Hur, "Anomalous thermal hysteresis in magnetization and resistivity of $La_{1-x}Sr_xMnO_3$," *Physical Review Letters*, vol. 87, no. 18, Article ID 187201, 2001.

[4] R. Desfeux, S. Bailleul, A. Da Costa, W. Prellier, and A. M. Haghiri-Gosnet, "Substrate effect on the magnetic microstructure of $La_{0.7}Sr_{0.3}MnO_3$ thin films studied by magnetic force microscopy," *Applied Physics Letters*, vol. 78, no. 23, pp. 3681–3683, 2001.

[5] R. Müller, W. Schüppel, T. Eick, H. Steinmetz, and E. Steinbeiß, "LaSr-manganate powders by crystallization of a borate glass," *Journal of Magnetism and Magnetic Materials*, vol. 217, no. 1, pp. 155–158, 2000.

[6] N. Kallel, K. Fröhlich, S. Pignard, M. Oumezzine, and H. Vincent, "Structure, magnetic and magnetoresistive properties of $La_{0.7}Sr_{0.3}MnO_3$ samples ($0 \le x \le 0.20$)," *Journal of Alloys and Compounds*, vol. 399, no. 1-2, pp. 20–26, 2005.

[7] K. S. Syed Ali, R. Saravanan, A. V. Pashchenko, and V. P. Pashchenko, "Local distortion in Co-doped LSMO from entropy-maximized charge density distribution," *Journal of Alloys and Compounds*, vol. 501, no. 2, pp. 307–312, 2010.

[8] H. Abdullah and M. S. Zulfakar, "Structural and surface morphology studies of $La_{0.67}Ba_{0.33}(Mn_{1-x}Al_x)O_3$ thin films prepared by sol-gel method," *Journal of Nanomaterials*, vol. 2013, Article ID 412741, 5 pages, 2013.

[9] H. Abdullah and S. A. Halim, "Electrical and microstructural properties of $(La_{1-x}Pr_x)_{1/2}Ba_{1/2}MnO_3$ compounds," *Sains Malaysiana*, vol. 38, no. 2, pp. 209–213, 2009.

[10] D. R. Sahu, B. K. Roul, P. Pramanik, and J.-L. Huang, "Synthesis of $La_{0.7}Sr_{0.3}MnO_3$ materials by versatile chemical technique," *Physica B*, vol. 369, no. 1–4, pp. 209–214, 2005.

[11] H. Abdullah, S. A. Halim, K. P. Lim, and A. N. Jannah, "Magneto-transport studies on $La_{2/3}Ba_{1/3}(Mn_{1-x}Al_x)O_3$ for low field sensing applications," *Materials Research Innovations*, vol. 13, no. 3, pp. 386–390, 2009.

[12] G. Venkataiah, D. C. Krishna, M. Vithal et al., "Effect of sintering temperature on electrical transport properties of $La_{0.67}Ca_{0.33}MnO_3$," *Physica B*, vol. 357, no. 3-4, pp. 370–379, 2005.

[13] H. Abdullah, S. A. Halim, and A. N. Jannah, "Effect of disorder particles size of Nd on electrical transport on a bulk of $Pr_{2/3}Ba_{1/3}MnO_3$," *Journal of Composite Materials*, vol. 46, no. 24, pp. 3103–3112, 2012.

[14] N. F. Mott, *Metal-Insulator Transition*, Taylor & Francis, 1999.

[15] W.-H. Jung, "Evaluation of Mott's parameters for hopping conduction in $La_{0.67}Ca_{0.33}MnO_3$ above Tc," *Journal of Materials Science Letters*, vol. 17, no. 15, pp. 1317–1319, 1998.

[16] S. Bhattacharya, R. K. Mukherjee, B. K. Chaudhuri, and H. D. Yang, "Effect of Li doping on the magnetotransport properties of $La_{0.7}Ca_{0.3\,y}Li_yMnO_3$ system: decrease of metal-insulator transition temperature," *Applied Physics Letters*, vol. 82, no. 23, pp. 4101–4103, 2003.

[17] S. L. Yuan, M. H. Liu, Z. Y. Li et al., "Effect of annealing temperature on electrical transport in $La_{2/3}Ca_{1/3}MnO_3$," *Solid State Communications*, vol. 121, no. 6-7, pp. 291–294, 2002.

[18] Y. Fu, Z. Zi, Q. Liu, Y. Cheng, and J. Dai, "$La_{0.6}Sr_{0.4}MnO_3$ particles synthesized under an external magnetic field," *Materials Letters*, vol. 71, pp. 41–43, 2012.

[19] D. C. Krishna and P. Venugopal Reddy, "Magnetic transport behavior of nano-crystalline $Pr_{0.67}A_{0.33}MnO_3$ (A = Ca, Sr, Pb and Ba) manganites," *Journal of Alloys and Compounds*, vol. 479, no. 1-2, pp. 661–669, 2009.